



# Geophysical Research Letters



## RESEARCH LETTER

10.1029/2019GL083306

### Special Section:

Bridging Weather and Climate: Subseasonal-to-Seasonal (S2S) Prediction

### Key Points:

- Record early and late anomalies in the timing of snowmelt in northern Alaska have been observed from 2015-2018
- Timing of snowmelt is linked to atmospheric transport of air masses from the north Pacific
- A climate index is introduced that is sensitive to the implicated advection and may be useful as a monitoring or prediction tool

### Supporting Information:

- Supporting Information S1

### Correspondence to:

C. J. Cox,  
christopher.j.cox@noaa.gov

### Citation:

Cox, C. J., Stone, R. S., Douglas, D. C., Stanitski, D. M., & Gallagher, M. R. (2019). The Aleutian Low-Beaufort Sea Anticyclone: A climate index correlated with the timing of springtime melt in the Pacific Arctic cryosphere. *Geophysical Research Letters*, *46*, 7464–7473. <https://doi.org/10.1029/2019GL083306>

Received 15 APR 2019

Accepted 8 JUN 2019

Accepted article online 14 JUN 2019

Published online 1 JUL 2019

©2019. The Authors.

This is an open access article under the terms of the Creative Commons Attribution-NonCommercial-NoDerivs License, which permits use and distribution in any medium, provided the original work is properly cited, the use is non-commercial and no modifications or adaptations are made.

## The Aleutian Low-Beaufort Sea Anticyclone: A Climate Index Correlated With the Timing of Springtime Melt in the Pacific Arctic Cryosphere

C. J. Cox<sup>1,2,3</sup> , R. S. Stone<sup>4,5</sup>, D. C. Douglas<sup>6</sup> , D. M. Stanitski<sup>7</sup> , and M. R. Gallagher<sup>1,2,3</sup>

<sup>1</sup>Cooperative Institute for Research in Environmental Sciences, Boulder, CO, USA, <sup>2</sup>NOAA Physical Sciences Division, Boulder, CO, USA, <sup>3</sup>University of Colorado Boulder, Boulder, CO, USA, <sup>4</sup>Science and Technology Corporation, Boulder, CO, USA, <sup>5</sup>Retired, NOAA Global Monitoring Division, Boulder, CO, USA, <sup>6</sup>U.S. Geological Survey Alaska Science Center, Juneau, AK, USA, <sup>7</sup>NOAA Global Monitoring Division, Boulder, CO, USA

**Abstract** Early and late extremes in the timing of snowmelt have recently been observed in the Pacific Arctic. Subseasonal-to-seasonal forecasts of this timing are important for industry, environmental management, and Arctic communities. In northern Alaska, the timing is influenced by the advection of marine air from the north Pacific by the Aleutian Low, modulated by high pressure centered in the Beaufort Sea. A new climate index that integrates their interaction could advance melt predictions. We define this index based on 850-hPa geopotential height at four fixed locations and refer to it as the Aleutian Low-Beaufort Sea Anticyclone (ALBSA). During positive ALBSA in May, advection of +0.5-1.5 K/day is observed through the Bering Strait. ALBSA is correlated with both snowmelt in northern Alaska and the onset of sea ice melt over the adjacent seas. ALBSA therefore may be suitable for monitoring the relevant circulation patterns and for developing predictive tools.

**Plain Language Summary** Early and late extremes in the timing of snowmelt have recently been observed in northern Alaska. Forecasts of this timing with lead times of weeks to months are important for area stakeholders including industry, environmental managers, and Arctic communities. We find that transport of air masses from the north Pacific influences the timing of melt in the region. We introduce a new index called the Aleutian Low-Beaufort Sea Anticyclone (ALBSA). When ALBSA is positive, warm Pacific air is observed over the Bering Strait and in the far western Arctic seas. ALBSA is correlated with the timing of spring melt and therefore may be suitable for both monitoring and prediction.

### 1. Introduction

Spring is a sensitive season for the Arctic terrestrial environment because snowmelt elicits responses in biogeochemical cycles, vegetation growth, ecology, soil temperature, and the surface energy budget (Cox et al., 2017, and references therein). Recent years have seen winter and spring climate extremes in the Pacific Arctic, including the 2016 winter heat wave (Overland & Wang, 2016; Walsh et al., 2017), and springtime warmth in 2015 and 2016 leading to the fourth and first earliest dates of snowmelt, respectively, recorded at Utqiagvik (formerly Barrow), Alaska (Cox et al., 2017). These events are consistent with anomalies in snow cover extent around the Pacific Arctic (Derksen et al., 2016, 2017). In 2015, the early melt was followed by widespread wildfires in central Alaska (Partain et al., 2016). A common feature of early melt is the transport of air from the north Pacific to the Arctic near the Bering Strait, an important gateway for air entering the Arctic from lower latitudes (Dufour et al., 2016). This transport is facilitated by the strength and position of the Aleutian Low (AL; Stone et al., 2002; Shulski et al., 2010; Walsh et al., 2017; Cox et al., 2017) and modulated by the Beaufort High (Ballinger et al., 2018; Cox et al., 2017; Stone et al., 2002). Such advection has been linked to preconditioning of sea ice (e.g., Kapsch et al., 2013), including onset of melt (Mortin et al., 2016) and the minimum sea ice extent in 2007 (Dong et al., 2014). However, circulation patterns during winter (Walsh et al., 2017) and spring (Cox et al., 2017) 2016 were different, suggesting complexity in the advection pathways.

A multidecadal warming trend has been documented across the North Slope of Alaska (NSA; Wendler et al., 2014) and the nearby ocean (Serreze et al., 2009). The latter has been linked to Arctic amplification in autumn and winter. Springtime warming has been less pronounced, however, and a trend toward earlier snowmelt dates at Utqiagvik is likely influenced by variability in atmospheric circulation patterns (Cox

et al., 2017; Stone et al., 2002). Indeed, a combination of factors contributed to the 2016 warmth, but circulation had greater importance at the end of the winter than at the beginning (Walsh et al., 2017).

Timing of springtime melt affects communities and industry, and there is a need for improved forecasting at subseasonal-to-seasonal time scales given the recent large interannual variability. We introduce a new regional climate index called the Aleutian Low-Beaufort Sea Anticyclone (ALBSA). ALBSA tracks the synergy among dominant regional pressure centers and is shown here to explain a significant amount of the variance in spring melt metrics over both the terrestrial and marine regions of the Pacific Arctic. ALBSA is suitable for monitoring the regional circulation that is influential to spring melt and may be useful for developing seasonal-scale predictive tools.

## 2. Data and Methods

Observations of snowmelt dates at Utqiagvik (Figure 1a) are available as early as 1902 (Cox et al., 2017), but we constrain the present analysis to 1979–2018 when other data sets of interest overlap. The methodology and historical records are described by Stone et al. (2002) and Cox et al. (2017). Dates reported from other stations (Kane & Hinzman, 2017) across the NSA are similarly derived. Surface melt onset over sea ice is derived from satellite passive microwave sensors (Markus et al., 2009), and the date of terrestrial snowmelt is based on the Northern Hemisphere Snow Cover Extent (NH-SCE) data set (Estilow et al., 2015). Melt dates from NH-SCE use the method of Choi et al. (2010), except snowfall events after the snowpack melted did not extend the snow season. NH-SCE dates agree with those at Utqiagvik in nearby grid cells beginning in the late 1970s (Cox et al., 2017). Near-surface air temperatures are from the NOAA observatory at Utqiagvik and from the U.S. Department of Energy (DoE) Atmospheric Radiation Measurement (ARM) Program at Oliktok Point (beg. 2013). For atmospheric circulation, we use daily mean 850-hPa geopotential heights (GPHs) from National Centers for Environmental Prediction–National Center for Atmospheric Research (NCEP–NCAR) Reanalysis (NNR; Kalnay et al., 1996). We constructed a 20-node, Self Organizing Map (SOM) from NNR sea level pressures in the Alaska region using the method of Gallagher et al. (2018) and mapped GPH and ALBSA onto the SOM to illustrate how ALBSA represents pressure patterns across the study area. We analyzed wavelet transforms (Cox et al., 2014; Torrence & Compo, 1998) and autocorrelations of the ALBSA time series to evaluate the temporal scale of ALBSA's potential forecasting capability.

## 3. Observed Variability in Snowmelt

The earliest snowmelt dates at Utqiagvik occur in mid-May, while the latest occur in late-June (Figure 1a). In contrast to the early melt in 2015 and 2016, 2017 and 2018 were the latest since 1988 and 1947, respectively. Although differences between consecutive years of at least 2 weeks occur ~10% of the time, the largest swing prior to 2016/2017 (35 days) was more than 100 years prior (1902/1903, 19 days).

Generally, snowmelt on the NSA progresses from the Brooks Range northward to Utqiagvik. This is evidenced by comparison to other regional measurements (Figures 1a and 1b), which show similar interannual variability supporting previous reports that Utqiagvik is representative (Cox et al., 2017; Stone et al., 2002).

Here we define years with “early” and “late” snowmelt as having anomalies larger than  $\pm 6$  days from the linearly detrended Utqiagvik time series, which is more restrictive than  $1\sigma$  (7.3 days) but identifies a similar number of early (6) and late (7) years (Figure 1a). From these, three early and three late years were selected as case studies for more detailed analysis. First, we focus on 2002 and 1988 because they are instructive examples of early versus late years, respectively, followed by 2015 through 2018, which represent extreme interannual shifts.

## 4. Aleutian Low-Beaufort Sea Anticyclone (ALBSA)

Guided by the case studies presented below, we developed ALBSA based on GPH at four geographic locations shown in Figures 2a and 2b. GPH at these coordinates are combined to create a single metric that is sensitive to the circulation patterns that promote early versus late years of snowmelt. ALBSA is formally defined in section 4.2, but first the case studies are presented to underpin ALBSA's construct. In section 4.3 we present a SOM to describe the circulation patterns to which ALBSA is most sensitive. In section 4.4 we examine statistical relationships in a 40-year time series of ALBSA and regional melt.

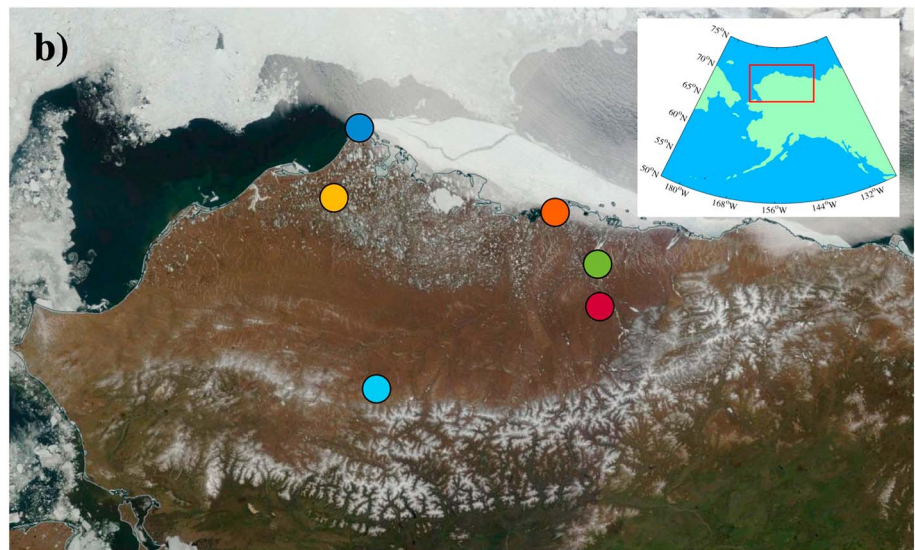
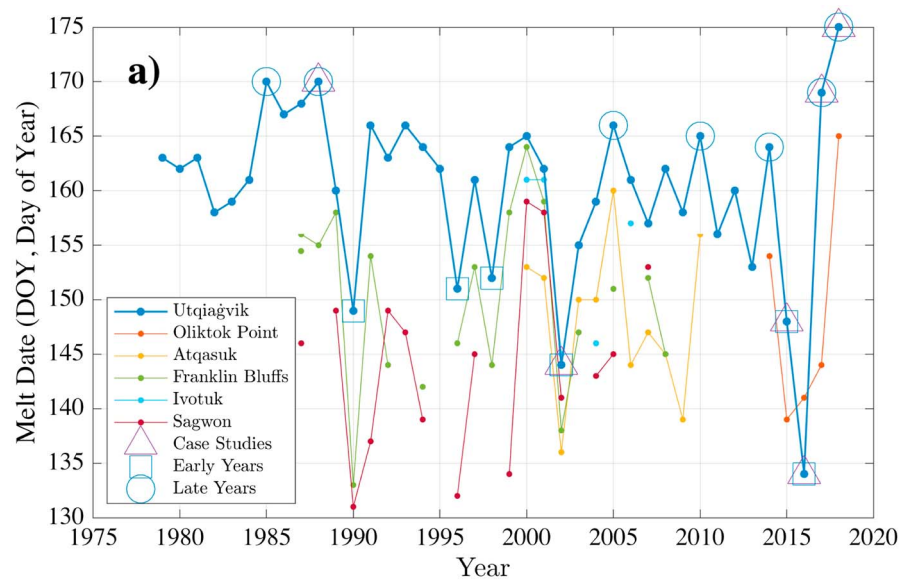


**Figure 1.** (a) Time series of snowmelt dates from Utqiagvik, 1979–2018 (blue), and available data from other nearby surface observatories. The blue circles are the seven late years (1985, 1988, 2005, 2010, 2014, 2017, and 2018), the blue squares are the six early years (1990, 1996, 1998, 2002, 2015, and 2016), and the purple triangles are the six case study years. (b) MODIS image (NASA Worldview, <https://worldview.earthdata.nasa.gov>) of the North Slope of Alaska region with the locations of the surface stations plotted in (a).

#### 4.1. Case Studies

Pacific Arctic circulation patterns for May 1988 and 2002 are shown in Figures 2a and 2b. These contrasting years are qualitatively similar to respective patterns based on aggregates of late and early snowmelt years shown previously (Cox et al., 2017). In spring 1988, the Beaufort Sea Anticyclone (BSA) was well developed north of Alaska and the AL was centered south of the Bering Sea (Figure 2a). Such a dipole pattern tends to block Pacific air from reaching the northern coast, thereby moderating temperatures as is evidenced by the 2-m air temperature measured at Utqiagvik (Figure 2g), which shows a steady seasonal increase with little variability from May into June. While synoptic cycles are observable in the time series, their amplitude is small and close to the climatological mean. Under these circumstances, the snowpack was preserved.

The May circulation pattern was notably different in 2002 (Figure 2b) when snow melted early. The AL was positioned farther west, allowing Pacific air to flow farther north through the Bering Strait (see also

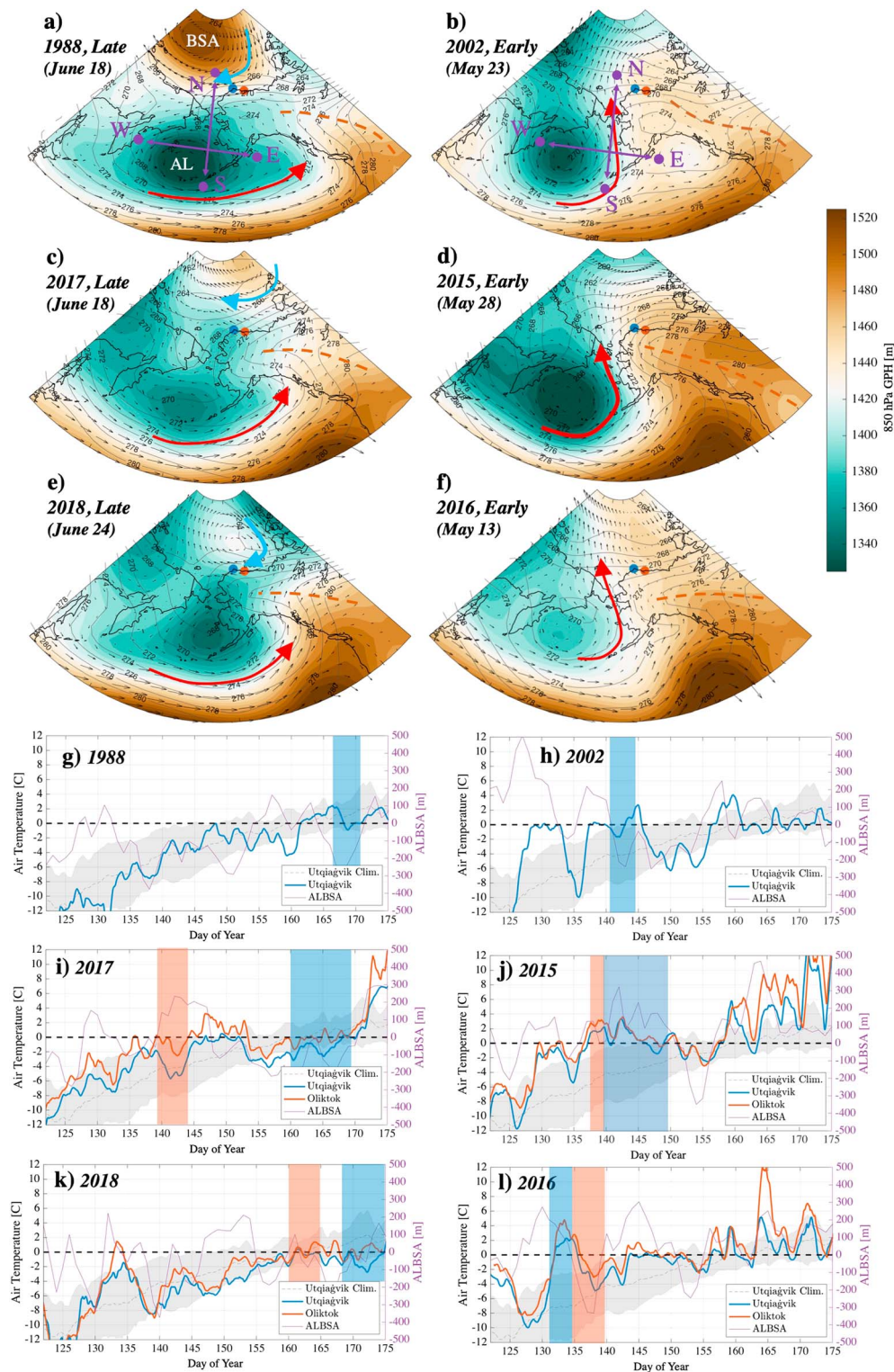


**Figure 2.** 850-hPa geopotential height averaged for May (solid contours) in (a) 1988, (b) 2002, (c) 2017, (d) 2015, (e) 2018, and (f) 2016. The open contours are air temperature, and the arrows are wind vectors at 850 hPa. The blue dot is Utqiagvik, and the red dot is Oliktok. Dates are the snowmelt date at Utqiagvik. The colored arrows illustrate the general direction of the air flow around the AL (red) and the BSA (blue). The dashed-brown line is the high-pressure ridge (HPR). Panels (a) and (b) show locations of the four Aleutian Low-Beaufort Sea Anticyclone (ALBSA) coordinates (purple; section 4.2). (g-l) Hourly 2-m air temperature smoothed with a 24-hr moving window May-June for years corresponding to (a)-(f), 2-m air temperature climatology (dashed) with  $\pm 1\sigma$  (shaded), and daily ALBSA (purple dots). The vertical bars show the snowmelt period defined as the period when daily mean albedo falls from 0.7 (melt onset) to 0.3 (melt complete) at Utqiagvik (blue) and Oliktok (red).

Figure S1 in the supporting information). To the east, a high-pressure ridge (HPR) extended north to the NSA, directing warm air into the Beaufort Sea. During early May, temperature anomalies (relative to climatology) of 5–12°C are required to reach the melting point; thus, large pulses of energy, or perhaps several (e.g., Persson, 2012), were needed to initiate melt. This was the case in May 2002, although temperatures were constrained to near 0 °C during melt. The first warm pulse occurred around days of year 128–133 (Figure 2h) followed by two more during which the snow melted rapidly and after which above-freezing temperatures persisted.

Circulation patterns during May 2017 and 2018 (Figures 2c and 2e) were similar to 1988. In spring 2017, the AL was positioned centrally, forming a north-south dipole with high pressure over the Beaufort Sea. Pacific air was directed away from northern Alaska due to blocking by the BSA, albeit weaker than during May 1988 (see also Figure S1). At times, air was advected farther north when low pressure extended toward Utqiagvik, while at the same time the HPR transported warm continental air farther to the east. At Oliktok Point, 250 km east of Utqiagvik, air temperatures during 2017 covaried with those at Utqiagvik but were warmer (red and blue lines in Figure 2i). There was enough warmth to melt snow at Oliktok, while it remained preserved for three more weeks at Utqiagvik (Figure 1a). This example illustrates how the spring transition can differ from east to west on Alaska's northern coast because the region is situated at the confluence of air masses transported by the AL, blocked by the BSA, and modulated by the HPR. Many of the same circulation features seen in 2017 occurred in 2018 (Figures 2e and 2k), in particular the central position of the AL and cool, dry air delivered to the NSA by the BSA.

During snowmelt in 2015 and 2016 (Figures 2d and 2f), the circulation patterns were similar to 2002 (Figure 2b). The main difference for 2016 was that the HPR extended farther north, blocking northeasterlies along the NSA. An intense heat wave caused by flow over the HPR during mid-May 2016 resulted in early melt at both Utqiagvik and Oliktok. In 2015 (Figure 2d and 2j), May conditions were similar to 2002 with a strong east to west pressure gradient that favored the flow of Pacific air northward, then eastward around the HPR across the NSA.

#### 4.2. ALBSA Defined

To represent the distinct meridional and zonal pressure gradients that underlie the early versus late years of snowmelt, ALBSA is defined at four points (Figures 2a and 2b) termed North (“N” at 75°N/170°W), South (“S” at 50°N/170°W), East (“E” at 55°N/150°W), and West (“W” at 55°N/160°E). The coordinates were selected to quantify pressure gradients along a *NS* transect spanning the north Pacific to the Chukchi Sea and an *EW* transect extending from the Kamchatka Peninsula to the Gulf of Alaska. It is the gradient in atmospheric pressure, or lack thereof, along these transects that determine if Pacific air masses flow into the Arctic and what trajectory they take. Of interest is variability at approximate cloud height, taken to be the 850-hPa level (Stone et al., 2002). Specifically, *EW* accounts for the strength and meridional position of the AL, while *NS* defines the pressure gradient between the BSA and points south of the AL central pressure based on climatology. The GPH pressure gradients are quantified as

$$NS = N - S, \quad (1)$$

$$EW = E - W. \quad (2)$$

Then, *NS* and *EW* are combined to produce the ALBSA index:

$$ALBSA = EW - NS. \quad (3)$$

#### 4.3. Visualizing ALBSA With a Self Organizing Map

To illustrate how ALBSA values relate to early and late years of snowmelt and regional circulation, the climatology of Pacific Arctic pressure patterns was ordinated on a SOM with twenty classes (“nodes”) akin to Ballinger et al. (2018). Composites of daily means of 850 hPa GPH for each of the nodes is shown in Figure 3a, highlighting the continuum of regional atmospheric circulation patterns. The two-dimensional arrangement of the matrix is exemplified by the SOM's orthogonal gradients: From the top-right (node 5) moving downward represents a transition from a strong BSA and westward positioned AL to a more centrally located AL and weak BSA. Moving left from node 5, the AL shifts to the west and the HPR forms to the east.

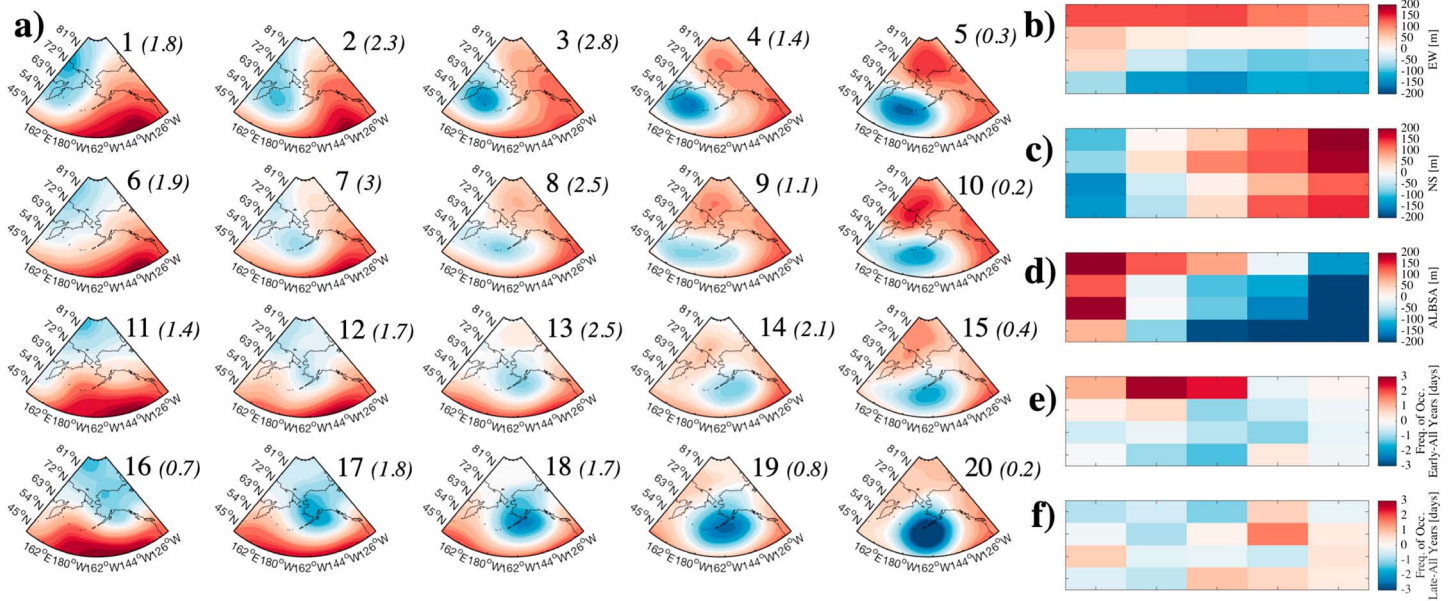


**Figure 3.** (a) 5×4 Self Organizing Map with each node numbered and the climatological frequency in days of the node during May in italics. Panels in (a) show the mean daily 850 hPa geopotential height for all days in May (1979-2018) that were classified to the respective Self Organizing Map node. (b) Average of *EW* (equation (2)) during May for each node, 1979-2017. (c) As in (b) but for *NS* (equation (1)) and (d) as in (a) and (b) but for *ALBSA* (equation (3)). (e and f) Mean frequencies [days] in May relative to May climatology of each node for early and late years (see Figure 1a), respectively.

Accordingly, the patterns in the upper left represent early years of snowmelt at Utqiagvik, while those representing late snowmelt appear near the middle and to the right. *EW* and *NS* components of *ALBSA* also conform with these orthogonal transitions. Nodes representing composite daily means of *EW* are positive along the top row and transition to negative values along the bottom row (Figure 3b), while positive values of *NS* are found on the right and negative values on the left (Figure 3c). The component sum, *ALBSA*, varies along the diagonal, with the largest positive value at node 1 and largest negative value at node 20 (Figure 3d). Therefore, the recognizable patterns from the case studies fall into distinctly positive values for early years of melt and negative values when melt is late. This organization provides context for interpreting the circulation states represented by values of *ALBSA*.

#### 4.4. *ALBSA*'s Relationship to Springtime Melt

Daily means of *ALBSA* are plotted in Figures 2g-2l (purple lines) showing that instances of increased (positive) *ALBSA*, corresponding to circulation patterns that are consistent with early melt, generally lead episodes of warm air observed at Utqiagvik by several days. However, these synoptic events are embedded within the storm track, the position of which varies with the planetary wave structure over time scales of 1-3 weeks (assuming a zonal wind propagation of 2-5 m/s at 850 hPa; Wallace, 2003). *ALBSA* is sensitive to this low-frequency variability, which represents a cycle in the probability of events tied to melt occurring in the region. Analysis of a wavelet transform of the *ALBSA* time series reveals a disproportionate amount of *ALBSA*'s variance in spring (March-April-May) is concentrated at periods of 1-3 weeks, peaking near 2 weeks (Figure 4a, red line). Persistence at these time scales is also apparent from the autocorrelation function (Figure S2), which shows significance as far as week 5. Thus, we should expect the melt date to be significantly correlated with *ALBSA* averaged for several weeks prior to snowmelt, as shown in Figure 4b for Utqiagvik. The correlation is negative meaning positive values of *ALBSA* precede early melt dates. Because of consistently negative values during April (not shown), 2016 is an outlier and counters the expected relationship. However, *ALBSA* was highly positive during May 2016 for 7 days prior to the melt date (green square in Figure 4b). The late melt in 2018 was preceded by less negative *ALBSA* than would be expected based on the other years. This is partially due to *ALBSA* transitioning to persistently positive values in June in tandem with the seasonal cycle of Northern Hemisphere circulation (e.g., Overland & Wang, 2016; Figure S3).

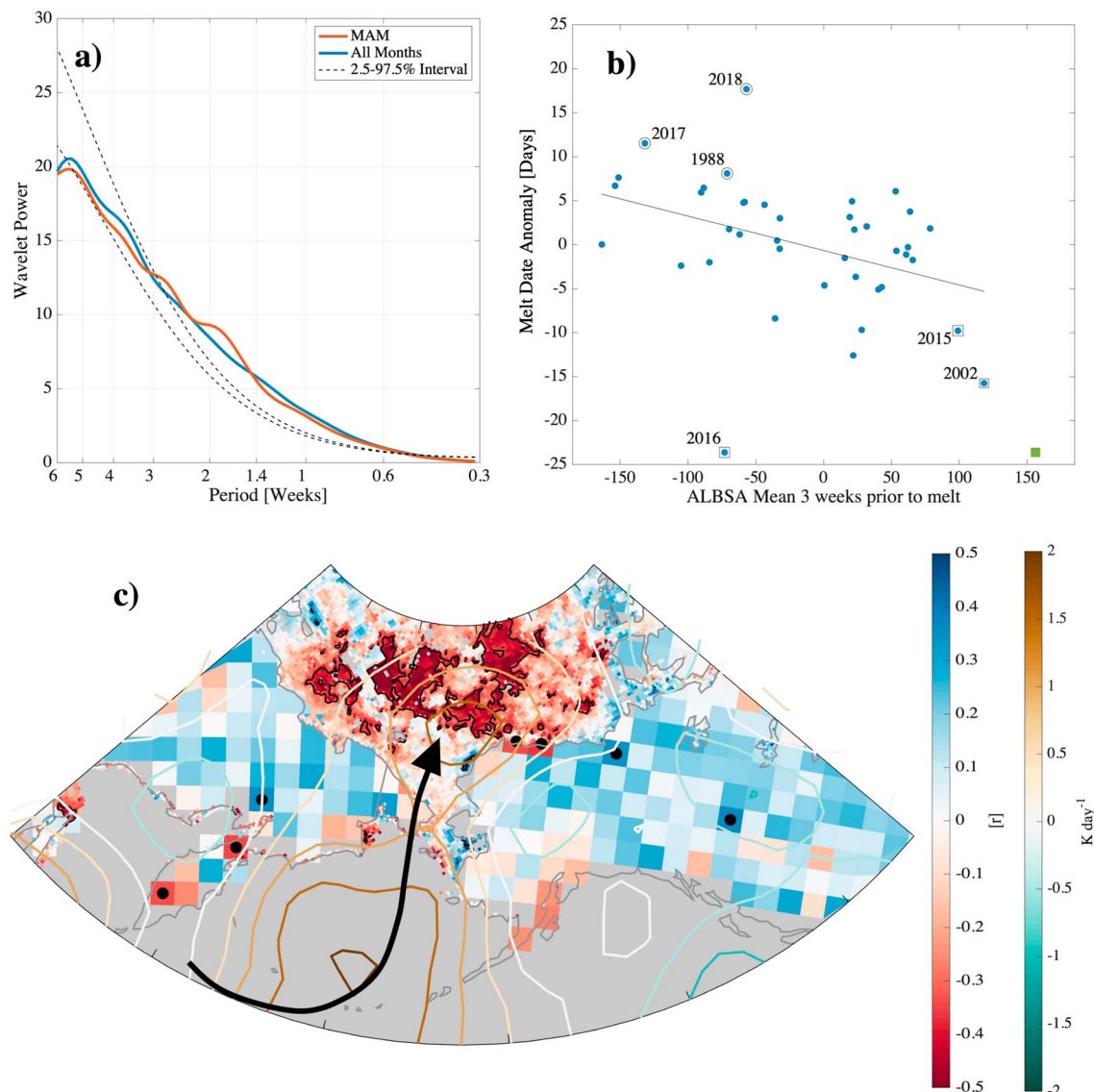


**Figure 4.** (a) Wavelet power spectra for periods of 0.3-6 weeks calculated from daily Aleutian Low-Beaufort Sea Anticyclone (ALBSA) values (1979-2018) averaged for all months (blue) and spring (March-April-May, red). The dashed lines are the 2.5%-97.5% confidence interval. (b) Linearly detrended melt date anomaly at Utqiagvik versus mean ALBSA averaged over 3 weeks prior to the melt date in each year. ALBSA was not detrended because no trend is detectable in the analyzed time series. The least absolute deviation regression slope is  $-0.04$  [days/meter ALBSA] ( $p = 0.01$ ;  $r = -0.38$  ( $-0.52$  if 2016 is omitted)). The green square is the ALBSA mean for 7 days prior to melt in 2016. Large annotated circles highlight case-study years. (c) Correlation ( $r$ ) between average May ALBSA and the timing of melt onset over sea ice (ocean pixels, 1979-2017) and the date of snowmelt over land (land pixels, 1979-2018). The black dots over land and black contours over sea ice mark pixels with statistically significant correlations nominally for  $p < 0.05$ , but adjusted to a stricter threshold of  $\sim 0.04$  to account for false discovery rates for tested pixels inside the domain (Wilks, 2016). The black arrow is the approximate path of advection in early melt years. Advection ( $u + v$ ) is shown (colored contours,  $\text{K day}^{-1}$ ) for days with ALBSA  $> +1\sigma$  based on all days in May, 1979-2018.

Circulation patterns in the upper left SOM (Figure 3a), especially nodes 2 and 3, are qualitatively similar to the early melt years in Figure 2. Correspondingly, days classified into these nodes occur more frequently during May in years of early melt (Figure 3e). Collectively, 8 to 20 days during May mapped into nodes 2 or 3 during early melt years, except in 1998 when May was instead dominated by other positive-ALBSA nodes (1, 6, and 7). While patterns in the lower-right SOM are generally more common during May in late years, there are no distinct late-melt patterns (Figure 3f). Therefore, late years may be best characterized as lacking circulation patterns that favor early melt.

During May, the mean net advection ( $u+v$ ) of temperature at 850 hPa when ALBSA is strongly positive ( $> +1\sigma$ ) shows warming from the North Pacific through the Bering Strait and into the Arctic (Figure 4c;

Figure S4 for the analogous plot for negative ALBSA). This is the result of northward transport of air ( $v$ ) from the AL along the HPR while the  $u$  component narrows the corridor. Once reaching the Arctic, the weak BSA allows the air to continue following the HPR eastward, over the NSA, where it can influence the snowpack. In contrast, much of interior Alaska shows neutral values of advected temperature, consistent with the lack of significance in the correlation with snow melt date in these areas, which are within the HPR and influenced by different air masses. Average May values of ALBSA are therefore negatively correlated with the timing of melt derived from satellite retrievals (Figure 4c, red shading) over an extensive region subject to the warm-air advection. Specifically, when ALBSA is positive in May, early onset of sea ice melt occurs over the East Siberian, Chukchi, and Beaufort Seas, as well as early snowmelt on the NSA, consistent with Stone et al. (2005).

Interestingly, ALBSA is correlated ( $p < 0.05$ ) with other common climate indices in May, including the Pacific North American index (e.g., Barnston & Livezey, 1987;  $r = -0.34$ ), the North Atlantic Oscillation (Barnston & Livezey, 1987;  $r = 0.36$ ), the Arctic Oscillation (Thompson & Wallace, 2000;  $r = 0.60$ ), and the North Pacific pattern (Trenberth & Hurrell, 1994;  $r = 0.54$ ). However, these indices do not correlate with Utqiagvik melt dates nor do they show widespread or significant correlations with melt onset over the western Arctic seas as does ALBSA.

## 5. Discussion and Conclusions

Extraordinarily early and late snowmelt anomalies in northern Alaska have been observed in recent years. We find that early melt is associated with air being advected from the north Pacific along the eastern flank of the AL through the Bering Strait. Conversely, the snowpack can be preserved by a lack of such advection or local blocking by the BSA. These findings are consistent with other studies that link advection, facilitated by these pressure centers, to temperature anomalies in Alaska (e.g., Ballinger et al., 2018; Hartmann & Wendler, 2005; Shulski et al., 2010; Walsh et al., 2017). To improve forecasts with lead times of weeks to possibly months, we developed the ALBSA index, which quantifies the synergy of these pressure centers based on 850-hPa GPHs measured at four geographic coordinates. Positive values of ALBSA lead periods of warmth on the NSA by several days, consistent with the transit time of advected air masses. However, ALBSA is sensitive to the position of the storm track that guides synoptic activity and varies with a period of 1-3 weeks. Therefore, the types of events that lead to melt become more or less probable for extended periods of time. When ALBSA is strongly positive ( $>+1\sigma$ ), reanalysis data show temperature advection of  $+0.5$  to  $+1.5$  K/day from the North Pacific through the Bering Strait into the Arctic. These air masses promote both snowmelt over northern Alaska and the onset of sea ice melt in the East Siberian, Chukchi, and Beaufort Seas. Thus, ALBSA is negatively correlated with the timing of annual melting in these areas.

Early melt is associated with specific atmospheric circulation patterns characterized by a westward position of the AL and relatively weak BSA and/or the northward extension of a high-pressure ridge that forms over eastern Alaska. As classified by the SOM, these patterns are about three times more common during May in years of early melt compared with late years. Conversely, in years with late melt we find generally negative values of ALBSA, but no distinctive circulation patterns. In keeping with Cassano et al. (2011), the identification of early-melt patterns suggests that forecast tools using pattern-organization techniques such as SOMs could increase forecast confidence in some years by identifying patterns (nodes) that are persistent early indicators (with respect to melt) or precursors to other nodes that have such attributes. This applies not only to the NSA and melt metrics but likely also to other climate and environmental metrics important to regional commerce, ecology, and biogeochemical cycles.

The contrasting extremes from 2015 through 2018 were generally consistent with other early and late years, but also expressed unique features, including a split anomaly between the eastern and western NSA in 2017 and an abrupt shift from negative to positive ALBSA just prior to the melt in 2016. These nuanced factors arise in part because the region is at the confluence of air circulating around multiple influential pressure systems. Thus, there are likely multiple pathways of advection that may express characteristic differences that influence the onset and rate of melting. Factors include cloud-radiative effects (e.g., Liu & Schweiger, 2017), precipitation (Cassano & Cassano, 2010), and precipitation type (Bieniek et al., 2018). More work is warranted to extend ALBSA's sensitivity to the range of patterns that occur when ALBSA is near neutral

(i.e., the upper-right and lower-left corners of the SOM in Figure 3a), which may be possible with a complementary index that sums rather than differences  $EW$  and  $NS$  in equation (3).

While ALBSA shows promise as a monitoring tool, more study will help to identify optimal lead times and quantify ALBSA's skill and stability as a predictor variable over time, especially given evidence of multidecadal changes in the properties of the AL (Gan et al., 2017) and BSA (Ballinger et al., 2014; Moore, 2012). Future studies should also explore applications in other months and endeavor to link ALBSA with oceanic variables, which also affect coastal temperatures (Wendler et al., 2014) and sea ice melt (Serreze et al., 2016).

#### Acknowledgments

Cox received support from the Arctic Research Program of the NOAA Climate Program Office and the U.S. Department of Energy (DoE) Atmospheric Systems Research (ASR) program (DE-SC0013306). Gallagher received support from the National Science Foundation grants PLR 1314156 and 1303879. NOAA Utqiagvik data are available from the NOAA Global Monitoring Division (GMD) at <https://www.esrl.noaa.gov/gmd/obop/brw/>. Data collected by the DoE ARM program at Oliktok Point and Atqasuk may be acquired from <https://www.arm.gov>. Melt dates from SMMR and SSM/I passive microwave data from Markus et al. (2009) are available at <https://neptune.gsfc.nasa.gov>. Northern Hemisphere Snow Cover Extent (NH-SCE) data (Estilow et al., 2015) are available from <https://gis.ncdc.noaa.gov/>. Data from Ivotok are available from the NSF Arctic Data Center (<https://doi.org/10.5065/D6G44NFV>). Data from Franklin Bluffs and Sagwon were acquired from the University of Alaska at Fairbanks (Kane & Hinzman, 2017), [http://ine.uaf.edu/werc/projects/NorthSlope/e\\_kuparuk/franklin\\_bluffs/franklin\\_bluffs.html](http://ine.uaf.edu/werc/projects/NorthSlope/e_kuparuk/franklin_bluffs/franklin_bluffs.html) and [http://ine.uaf.edu/werc/projects/NorthSlope/e\\_kuparuk/sagwon/sagwon.html](http://ine.uaf.edu/werc/projects/NorthSlope/e_kuparuk/sagwon/sagwon.html). Monthly and daily mean indices of ALBSA are available from NOAA at <https://www.esrl.noaa.gov/psd/data/timeseries/ALBSA/>. The authors appreciate the efforts of Catherine Smith (CIRES) who maintains the ALBSA index online and useful conversations on atmospheric circulation with William Neff (CIRES), SOMs with Matthew Shupe (CIRES), Oliktok Point with Gijs de Boer (CIRES), and statistical analyses with Gilbert Compo (CIRES) and Laura Slivinski (CIRES), as well as an internal review by Compo and constructive comments provided by two anonymous reviewers.

#### References

- Ballinger, T. J., Lee, C. C., Sheridan, S. C., Crawford, A. D., Overland, J. E., & Wang, M. (2018). Subseasonal atmospheric regimes and ocean background forcing of Pacific Arctic sea ice melt onset. *Climate Dynamics*, 52(9-10), 5657–5672. <https://doi.org/10.1007/s00382-018-4467-x>
- Ballinger, T. J., Sheridan, S. C., & Hanna, E. (2014). Resolving the Beaufort Sea High using synoptic climatological methods. *International Journal of Climatology*, 34(11), 3312–3319. <https://doi.org/10.1002/joc.3907>
- Barnston, A. G., & Livezey, R. E. (1987). Classification, seasonality and persistence of low-frequency atmospheric circulation patterns. *Monthly Weather Review*, 115, 1083–1126. [https://doi.org/10.1175/1520-0493\(1987\)115<1083:CSAPOL>2.0.CO;2](https://doi.org/10.1175/1520-0493(1987)115<1083:CSAPOL>2.0.CO;2)
- Bieniek, P. A., Bhatt, U. S., Walsh, J. E., Lader, R., Griffith, B., Roach, J. K., & Thoman, R. L. (2018). Assessment of Alaska rain-on-snow events using dynamical downscaling. *Journal of Applied Meteorology and Climatology*, 57, 1847–1863. <https://doi.org/10.1175/JAMC-D-17-0276.1>
- Cassano, E. N., & Cassano, J. J. (2010). Synoptic forcing of precipitation in the Mackenzie and Yukon River basins. *International Journal of Climatology*, 30, 658–674. <https://doi.org/10.1002/joc.1926>
- Cassano, E. N., Cassano, J. J., & Nolan, M. (2011). Synoptic weather pattern controls on temperature. *Journal of Geophysical Research*, 116, D11108. <https://doi.org/10.1029/2010JD015341>
- Choi, G., Robinson, D. A., & Kang, S. (2010). Changing Northern Hemisphere snow seasons. *Journal of Climate*, 23, 5305–5310. <https://doi.org/10.1175/2010JCLI3644.1>
- Cox, C. J., Stone, R. S., Douglas, D. C., Stanitski, D. M., Divoky, G. J., Dutton, G. S., et al. (2017). Drivers and environmental responses to the changing annual snow cycle of northern Alaska. *Bulletin of the American Meteorological Society*, 98, 2559–2577. <https://doi.org/10.1175/BAMS-D-16-0201.1>
- Cox, C. J., Walden, V. P., Compo, G. P., Rowe, P. M., Shupe, M. D., & Steffen, K. (2014). Downwelling longwave flux over Summit, Greenland, 2010–2012: Analysis of surface-based observations and evaluation of ERA-Interim using wavelets. *Journal of Geophysical Research: Atmospheres*, 119, 12,317–12,337. <https://doi.org/10.1002/2014JD021975>
- Derksen, C., Brown, R., Mudryk, L., & Luojus, K. (2016). Terrestrial snow cover [in “State of the Climate in 2015”]. *Bulletin of the American Meteorological Society*, 97, S145–S149. <https://doi.org/10.1175/2016BAMSStateoftheClimate.1>
- Derksen, C., Brown, R., Mudryk, L., & Luojus, K. (2017). Terrestrial snow cover [in “State of the Climate in 2016”]. *Bulletin of the American Meteorological Society*, 98, S143–S145. <https://doi.org/10.1175/2017BAMSStateoftheClimate.1>
- Dong, X., Zib, B. J., Xi, B., Stanfield, R., Deng, Y., Zhang, X., et al. (2014). Critical mechanisms for the formation of extreme arctic sea-ice extent in the summers of 2007 and 1996. *Climate Dynamics*, 43, 53–70. <https://doi.org/10.1007/s000382-013-1920-8>
- Dufour, A., Zolina, O., & Gulev, S. K. (2016). Atmospheric moisture transport to the Arctic: Assessment of reanalyses and analysis of transport components. *Journal of Climate*, 29, 5061–5081. <https://doi.org/10.1175/JCLI-D-15-0559.1>
- Estilow, T. W., Young, A. H., & Robinson, D. A. (2015). A long-term Northern Hemisphere snow cover extent data record for climate studies and monitoring. *Earth System Science Data*, 7, 137–142. <https://doi.org/10.5194/essd-7-137-2015>
- Gallagher, M. R., Shupe, M. D., & Miller, N. B. (2018). Impact of atmospheric circulation on temperature, clouds, and radiation at Summit Station, Greenland, with Self Organizing Maps. *Journal of Climate*, 31(21), 8895–8915. <https://doi.org/10.1175/JCLI-D-17-0893.1>
- Gan, B., Wu, L., Jai, F., Li, S., Cai, W., Nakamura, H., et al. (2017). On the response of the Aleutian Low to Greenhouse warming. *Journal of Climate*, 30, 3907–3925. <https://doi.org/10.1175/JCLI-D-15-0789.1>
- Hartmann, B., & Wendler, G. (2005). The significance of the 1976 Pacific climate shift in the climatology of Alaska. *Journal of Climate*, 18, 4821–4839. <https://doi.org/10.1175/JCLI3532.1>
- Kalnay, E., Kanamitsu, M., Kistler, R., Collins, W., Deaven, D., Gandin, L., et al. (1996). The NCEP/NCAR 40-Year Reanalysis Project. *Bulletin of the American Meteorological Society*, 77, 437–472. [https://doi.org/10.1175/1520-0477\(1996\)077<0437:TNYRP>2.0.CO;2](https://doi.org/10.1175/1520-0477(1996)077<0437:TNYRP>2.0.CO;2)
- Kane, D. L. & Hinzman, L. D. (2017). Climate data from the North Slope Hydrology Research project. University of Alaska, Fairbanks, Water and Environmental Research Center. <http://ine.uaf.edu/werc/projects/NorthSlope/> Fairbanks, Alaska, variously paged.
- Kapsch, M.-L., Graversen, R. G., & Tjernström, M. (2013). Springtime atmospheric energy transport and the control of Arctic summer sea ice extent. *Nature Climate Change*, 3, 744–748. <https://doi.org/10.1038/nclimate1884>
- Liu, Z., & Schweiger, A. (2017). Synoptic conditions, clouds, and sea ice melt onset in the Beaufort and Chukchi seasonal ice zone. *Journal of Climate*, 30, 6999–7016. <https://doi.org/10.1175/JCLI-D-16-0887.1>
- Markus, T., Stroeve, J. C., & Miller, J. (2009). Recent changes in Arctic sea ice melt onset, freezeup, and melt season length. *Journal of Geophysical Research*, 114, C12024. <https://doi.org/10.1029/2009JC005436>
- Moore, G. W. K. (2012). Decadal variability and recent amplification of the summer Beaufort Sea High. *Geophysical Research Letters*, 39, L18087. <https://doi.org/10.1029/2012GL051570>
- Mortin, J., Svensson, G., Graversen, R. G., Kapsch, M.-L., Stroeve, J. C., & Boisert, L. N. (2016). Melt onset over Arctic sea ice controlled by atmospheric moisture transport. *Geophysical Research Letters*, 43, 6636–6642. <https://doi.org/10.1002/2016GL069330>
- Overland, J. E., & Wang, M. (2016). Recent extreme Arctic temperatures are due to a split polar vortex. *Journal of Climate*, 29, 5609–5616. <https://doi.org/10.1075/JCLI-D-16-0320.1>
- Partain, L. J., Alden, S., Strader, H., Bhatt, U. S., Bieniek, P. A., Brettschneider, B. R., et al. (2016). An assessment of the role of anthropogenic climate change in the Alaska fire season of 2015 [in “Explaining Extremes of 2015 from a Climate Perspective”]. *Bulletin of the American Meteorological Society*, 97, S14–S18. <https://doi.org/10.1175/BAMS-D-16-0149>

- Persson, P. O. G. (2012). Onset and end of the summer melt season over sea ice: Thermal structure and surface perspective from SHEBA. *Climate Dynamics*, 39, 1349–1371. <https://doi.org/10.1007/s00382-012-1349-1>
- Serreze, M., Barrett, A. P., Stroeve, J. C., Kindig, D. N., & Holland, M. M. (2009). The emergence of surface-based Arctic amplification. *The Cryosphere*, 3, 11–19. <https://doi.org/10.5194/tc-3-11-2009>
- Serreze, M., Crawford, A. D., Stroeve, J. C., Barrett, A. P., & Woodgate, R. A. (2016). Variability, trends, and predictability of seasonal sea ice retreat and advance in the Chukchi Sea. *Journal of Geophysical Research: Oceans*, 121, 7308–7325. <https://doi.org/10.1002/2016JC011977>
- Shulski, M., Walsh, J., Stevens, E., & Thoman, R. (2010). Diagnosis of extended cold-season temperature anomalies in Alaska. *Monthly Weather Review*, 138, 453–462. <https://doi.org/10.1175/2009MWR3039.1>
- Stone, R. S., Douglas, D., Belchansky, G., & Drobot, S. (2005). Correlated declines in Pacific arctic snow and sea ice cover. *Arctic Research of the United States*, 19, 18–25.
- Stone, R. S., Dutton, E. G., Harris, J. M., & Longenecker, D. (2002). Earlier spring snowmelt in northern Alaska as an indicator of climate change. *Journal of Geophysical Research*, 107(D10), 4089. <https://doi.org/10.1029/2000JD000286>
- Thompson, D. W. J., & Wallace, J. M. (2000). Annular modes in the extratropical circulation. Part 1: Month-to-month variability. *Journal of Climate*, 13, 1000–1016. [https://doi.org/10.1175/1520-0442\(2000\)013<1000:AMITEC>2.0.CO;2](https://doi.org/10.1175/1520-0442(2000)013<1000:AMITEC>2.0.CO;2)
- Torrence, C., & Compo, G. P. (1998). A practical guide to wavelet analysis. *Bulletin of the American Meteorological Society*, 79, 61–78. [https://doi.org/10.1175/1520-0477\(1998\)079<0061:APGTWA>2.0.CO;2](https://doi.org/10.1175/1520-0477(1998)079<0061:APGTWA>2.0.CO;2)
- Trenberth, K. E., & Hurrell, J. W. (1994). Decadal atmosphere-ocean variations in the Pacific. *Climate Dynamics*, 9, 303–319. <https://doi.org/10.1007/BF00204745>
- Wallace, J. M. (2003). General circulation: Overview. In J. R. Holton, J. A. Curry, & J. A. Pyle (Eds.), *Encyclopedia of atmospheric sciences* (pp. 821–829). London: Academic Press. <https://doi.org/10.1016/B978-0-12-382225-3.0015205>
- Walsh, J. E., Bieniek, P. A., Brettschneider, B., Euskirchen, E. S., Lader, R., & Thoman, R. L. (2017). The exceptionally warm winter of 2015/16 in Alaska. *Journal of Climate*, 30, 2069–2088. <https://doi.org/10.1175/JCLI-D-16-0473.1>
- Wendler, G., Morre, B., & Galloway, K. (2014). Strong temperature increase and shrinking sea ice in Arctic Alaska. *The Open Atmospheric Science Journal*, 8, 7–15. <https://doi.org/10.2174/1874282301408010007>
- Wilks, D. S. (2016). “The stippling show statistically significant grid points”: How research results are routinely overstated and overinterpreted, and what to do about it. *Bulletin of the American Meteorological Society*, 97, 2263–2273. <https://doi.org/10.1175/BAMS-D-15-00267.1>